MATHEMATICAL BIOSCIENCES
AND ENGINEERING
Volume **6**, Number **3**, July **2009**

doi:10.3934/mbe.2009.6.611

pp. **611–627**

# THEORETICAL MODELING OF RF ABLATION WITH INTERNALLY COOLED ELECTRODES: COMPARATIVE STUDY OF DIFFERENT THERMAL BOUNDARY CONDITIONS AT THE ELECTRODE-TISSUE INTERFACE

María J. Rivera, Juan A. López Molina and Macarena Trujillo

Instituto Universitario de Matemática Pura y Aplicada
Universidad Politécnica de Valencia
Camino de Vera s/n. 46022, Valencia, Spain

Enrique J. Berjano

Institute for Research and Innovation on Bioengineering
Universidad Politécnica de Valencia
Camino de Vera s/n. 46022, Valencia, Spain

(Communicated by Qing Nie)

Abstract. Previous studies on computer modeling of RF ablation with cooled electrodes modeled the internal cooling circuit by setting surface temperature at the coolant temperature (i.e., Dirichlet condition, DC). Our objective was to compare the temperature profiles computed from different thermal boundary conditions at the electrode-tissue interface. We built an analytical one-dimensional model based on a spherical electrode. Four cases were considered: A) DC with uniform initial condition, B) DC with pre-cooling period, C) Boundary condition based on Newton's cooling law (NC) with uniform initial condition, and D) NC with a pre-cooling period. The results showed that for a long time (120 s), the profiles obtained with (Cases B and D) and without (Cases A and C) considering pre-cooling are very similar. However, for shorter times ($< 30$ s), Cases A and C overestimated the temperature at points away from the electrode-tissue interface. In the NC cases, this overestimation was more evident for higher values of the convective heat transfer coefficient ($h$). Finally, with NC, when $h$ was increased the temperature profiles became more similar to those with DC. The results suggest that theoretical modeling of RF ablation with cooled electrodes should consider: 1) the modeling of a pre-cooling period, especially if one is interested in the thermal profiles registered at the beginning of RF application; and 2) NC rather than DC, especially for low flow in the internal circuit.

1. **Introduction.** Internally cooled electrodes (also known as *cooled-tip* electrodes, *actively cooled* electrodes or simply *cooled* electrodes) have been employed for delivering radiofrequency (RF) currents into biological tissue in different minimally invasive techniques such as ablation of cardiac arrhythmias [4, 15] and tumor ablation [12, 17]. Briefly, a closed-circuit internal irrigation system allows cooled liquid

2000 *Mathematics Subject Classification.* Primary: 92C05, 92C10, 92C50; Secondary: 93A30.
*Key words and phrases.* cardiac ablation, cooled electrode, radiofrequency ablation.
This work received financial support from the Spanish "Plan Nacional de Investigación Científica, Desarrollo e Innovación Tecnológica del Ministerio de Educación y Ciencia" (TEC2008-01369/TEC.) and from the MEC Project MTM2007-64222.

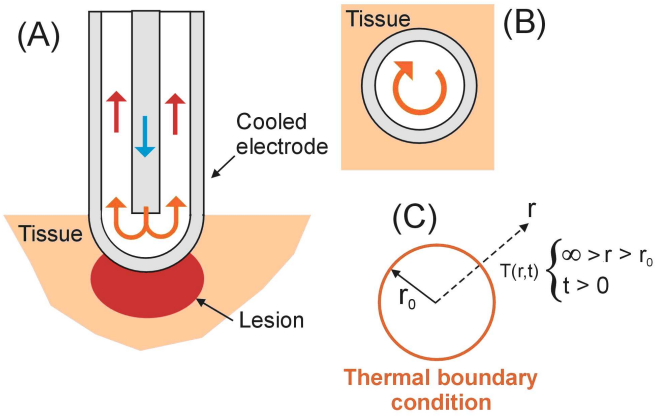


FIGURE 1. A: Physical situation for radiofrequency ablation with an internally cooled semispherical electrode. B: Simplification based on considering a spherical electrode completely imbedded and in close contact with the biological tissue, which has an infinite dimension. C: Theoretical model used in our study, which has radial symmetry, and hence a one-dimensional approach is possible (dimensional variable is $r$, and the electrode radius is $r_0$). The different thermal boundary conditions are applied on the outer circular boundary of the electrode.

circulation inside the electrode (see Fig. 1A). In comparison with dry electrodes (i.e., those without any kind of cooling), cooled electrodes allow lesion volume to be enlarged, which is always useful in cardiac and tumor ablation. It is important to point out that cooled electrodes are radically different to the irrigated type, in which saline is infused from the electrode to the exterior through perforations [8] (i.e., there is no close-loop hydraulic circuit). Cooled and irrigated electrodes can also be combined to form hybrid RF applicators [3].

Previous computer modeling studies have been carried out on cardiac [11, 14] and tumor [6]-[9] RF ablation using cooled electrodes. However, all of these modeled the internal cooling circuit by setting surface temperature at the coolant temperature, i.e. they employed a Dirichlet thermal boundary condition. This approach involves a simplification of the true physical situation, which has not been previously assessed. In fact, the use of other thermal boundary conditions (e.g. convective boundary condition) could produce different results. Our objective was to compare the temperature profiles computed from different thermal boundary conditions at the electrode-tissue interface for the particular case of RF cardiac ablation.

## 2. **Methods.**

### 2.1. **Description of the theoretical model.**

Figure 1B makes clear the simplification of the true physical situation as shown in Figure 1A. Briefly, we considered a spherical electrode completely imbedded and in close contact with the biological tissue, which had an infinite dimension. This model is similar to those proposed by Erez and Shitzer [7]. The model thus presented radial symmetry and a one-dimensional approach was possible (dimensional variable is $r$).

2.2. **Governing equations.** The RF ablation modeling implies an electrical-thermal coupled problem [1]. Regarding the electrical problem, the source term (i.e. the Joule heat produced per unit volume of tissue, $Q(r,t)$) can be expressed as:

$$Q(r,t) = \frac{P\, r_0}{4\pi r^4}\ (H(t) - H(t-\Delta t)) \tag{1}$$

where $P$ is the total applied power (W), $r_0$ the electrode radius (m), $H(t)$ is the Heaviside function, and $\Delta t$ is the pulse width (for RF application). Here we are modeling a constant power protocol, as is usually employed with cooled electrodes [15].

Regarding the thermal problem, we used the *Bioheat Equation* particularized to the case of RF cardiac ablation, in which the blood perfusion and metabolic heat were ignored [1]. For the one-dimensional case, this equation can be expressed as

$$-\alpha\left(\frac{\partial^2 T}{\partial r^2}(r,t) + \frac{2}{r}\,\frac{\partial T}{\partial r}(r,t)\right) + \frac{\partial T}{\partial t}(r,t) = \frac{P\ \alpha\ r_0}{4\ \pi\ k\ r^4}\ \Big(H(t) - H(t-\Delta t)\Big) \tag{2}$$

where $T$ is the temperature, $\alpha$ is the thermal diffusivity, and $k$ is thermal conductivity.

2.3. **Boundary thermal conditions at the electrode-tissue interface.** Previous studies on dry electrodes have modeled the thermal behavior at the electrode-tissue interface (i.e. in $r = r_0$) by assuming that the boundary condition at this point is mainly governed by the thermal inertia of the electrode [7, 13]. Since the thermal conductivity of the electrode ($k_0$) is much greater than that of the tissue, the following expression was obtained:

$$\rho_0\ c_0 \frac{4\ \pi\ r_0^3}{3}\ \frac{\partial T}{\partial t}(r_0,t) = 4\ \pi\ r_0^2\ k\ \frac{\partial T}{\partial r}(r_0,t) \tag{3}$$

where $\rho_0$ and $c_0$ are, respectively, the density and specific heat of the electrode.

Regarding the cooled electrodes, all previous modeling studies employed a Dirichlet thermal boundary condition in which the temperature at the electrode-tissue interface was fixed to the value at the coolant temperature ($T_c$)

$$T(r_0,t) = T_c\ . \tag{4}$$

Equation (4) is only a first approximation to the cooled electrode model, which induced us to consider other ways of modeling thermal behavior at the electrode-tissue interface. Another boundary condition is established from Newton's cooling law

$$q(r_0,t) = h(T_c - T(r_0,t))$$

where $h$ is the convective heat transfer coefficient and $q$ the heat flux. Since from Fourier's law $q(r_0,t) = -k\frac{\partial T}{\partial r}(r_0,t)$, then the boundary condition is

$$-\,k\frac{\partial T}{\partial r}(r_0,t) = h(T_c - T(r_0,t))\,. \tag{5}$$

The two above-mentioned thermal boundary conditions (i.e., equations (4) and (5)), employed the same complementary thermal condition:

$$\lim_{r\to\infty} T(r,t) = T_0 \tag{6}$$

where $T_0$ is the temperature of the non heated tissue (37°C).

We had two options for the initial conditions: on one hand, a uniform value equal to the temperature of the non heated tissue:

$$T(r,0) = T_0 \,. \tag{7}$$

On the other hand, to increase the accuracy of the theoretical modeling, we had the option of a more realistic approach in modeling the cooled electrodes. Cooled electrodes are cooled prior to RF power delivery, i.e. RF application is initiated after liquid irrigation reduces the temperature measured in the electrode (e.g. to a value of 32°C [4]). In order to model this situation, we first considered the following governing equation which is capable of modeling a sufficiently long pre-cooling period:

$$T''(r) + \frac{2}{r}\, T'(r) = 0\,. \tag{8}$$

Here the heat term source was removed to model the pre-cooling period without RF power delivery, and we also considered the steady-state situation, i.e., equation (8) was solved for two cases of boundary conditions at $r_0$ (eq. (4) and (5)). Once the thermal profile ($T(r)$) had been obtained from (8), this was employed as the initial condition instead of (7) to solve governing equation (2). Consequently, we considered four cases:

- *Case A*: Dirichlet boundary condition (eq. 4) with uniform initial condition (eq. 7).
- *Case B*: Dirichlet boundary condition (eq. 4) with a pre-cooling period (eq. 8).
- *Case C*: Boundary condition based on Newton's cooling law (eq. 5) with uniform initial condition (eq. 7).
- *Case D*: Boundary condition based on Newton's cooling law (eq. 5) with modeling a pre-cooling period (eq. 8).

The general purpose of this study was to compare the different temperature profiles obtained from the above four cases. We particularized our study for the case of a RF cardiac ablation in which a 7 Fr electrode is employed. We therefore considered a value of $r_0$ of 1.5 mm, coolant temperature ($T_c$) of 5°C, and a pulse width ($\Delta t$) of 120 s. For $h$, we considered three values: 1000, 2000 and 4000 W/m$^2$K, which correspond to forced thermal convection. Our objective was not to consider $h$ values which accurately matched the real values, but only to study the effect of varying this parameter, so temperature profiles were assessed both during heating (when RF power is applied) and subsequently. In all the cases we employed a power of 3 W, as in previous analytical study with dry electrodes [13]. We could therefore compare the temperature profiles obtained from cooled and dry electrodes. We also used the same tissue characteristics as had been previously considered [13]: density ($\rho$) of 1200 kg/m$^3$, specific heat ($c$) of 3200 J/kg·K, and thermal conductivity ($k$) of 0.70 W/m·K.

When the analytical solution had been obtained, we plotted the dimensional temperature distribution using Mathematica 5.2 software (Wolfram Research, Inc. Champaign, IL, USA).

## 3. Analytical results.

### 3.1. Case A: Dirichlet boundary condition and uniform initial condition.

Firstly we solve the problem formulated as the governing equation (2) with conditions (4), (6) and (7). In order to simplify the solution of the problem we shall make the following change of variables

$$\rho = \frac{r}{r_0}\ ; \qquad \xi = \frac{t\,\alpha}{r_0^2}\ ; \qquad V(\rho,\xi) = \frac{4\pi k r_0}{P}\left(T\left(r_0\rho, \frac{r_0^2\xi}{\alpha}\right) - T_0\right)\ ; \quad (9)$$

in this way the resulting problem is

$$-\left(\frac{\partial^2 V}{\partial\rho^2}(\rho,\xi) + \frac{2}{\rho}\frac{\partial V}{\partial\rho}(\rho,\xi)\right) + \frac{\partial V}{\partial\xi}(\rho,\xi) = \frac{1}{\rho^4}\left(H(\xi) - H(\xi-\Delta\xi)\right) \quad (10)$$

$$V(\rho,0) = 0 \qquad \forall\ \rho > 1 \quad (11)$$

$$\lim_{\rho\to\infty} V(\rho,\xi) = 0 \qquad \forall\ \xi > 0 \quad (12)$$

$$V(1,\xi) = -B \qquad \forall\ \xi > 0 \quad (13)$$

where $B = \frac{4\pi k r_0}{P}\,(T_0 - T_c)$.

Taking Laplace transform respect to $\xi$ and denoting $D(\rho,s) := \mathcal{L}(V(\rho,\xi))$ we get

$$-\left(\frac{\partial^2 D}{\partial\rho^2} + \frac{2}{\rho}\frac{\partial D}{\partial\rho}\right) + s\ D = \frac{1}{\rho^4}\left(\frac{1-e^{-s\Delta\xi}}{s}\right) \quad (14)$$

$$\lim_{\rho\to\infty} D(\rho,s) = 0 \quad (15)$$

$$D(1,s) = -\frac{B}{s}\ . \quad (16)$$

(14) is a second order differential equation. Using the new function $z(\rho,s) = \rho\ D(\rho,s)$ this equation becomes

$$-\frac{\partial^2 z}{\partial\rho^2} + sz = \frac{1}{\rho^3}\left(\frac{1-e^{-s\Delta\xi}}{s}\right) \quad (17)$$

whose solution is

$$z(\rho,s) = C_1(\rho,s)\ e^{\rho\sqrt{s}} + C_2(\rho,s)\ e^{-\rho\sqrt{s}}\ . \quad (18)$$

To determine $C_1(\rho,s)$ and $C_2(\rho,s)$ we use the variation of constants method. In this way taking into account the change of function we obtain

$$D(\rho,s) = \left(-\frac{1-e^{-\Delta\xi s}}{2s\sqrt{s}}\int_1^\rho \frac{e^{-u\sqrt{s}}}{u^3}\,du + M_1(s)\right)\frac{e^{\rho\sqrt{s}}}{\rho} + \left(\frac{1-e^{-\Delta\xi s}}{2s\sqrt{s}}\int_1^\rho \frac{e^{u\sqrt{s}}}{u^3}\,du + M_2(s)\right)\frac{e^{-\rho\sqrt{s}}}{\rho}\ . \quad (19)$$

The expressions of $M_1(s)$ and $M_2(s)$ are obtained from the boundary conditions. From condition (15) we have to determine $M_1(s)$ in order to verify

$$\lim_{\rho\to\infty}\left(-\frac{1-e^{-\Delta\xi s}}{2s\sqrt{s}}\int_1^\rho \frac{e^{-u\sqrt{s}}}{u^3}\,du + M_1(s)\right)\frac{e^{\rho\sqrt{s}}}{\rho} = 0\ .$$

In this way the expression of $M_1(s)$ is

$$M_1(s) = \frac{1-e^{-\Delta\xi s}}{2s\sqrt{s}} \int_1^\infty \frac{e^{-u\sqrt{s}}}{u^3}\, du\,, \tag{20}$$

since equation (19) becomes

$$D(\rho,s) = \left(\frac{1-e^{-\Delta\xi s}}{2s\sqrt{s}} \int_\rho^\infty \frac{e^{-u\sqrt{s}}}{u^3}\, du\right) \frac{e^{\rho\sqrt{s}}}{\rho} + \left(\frac{1-e^{-\Delta\xi s}}{2s\sqrt{s}} \int_1^\rho \frac{e^{u\sqrt{s}}}{u^3}\, du + M_2(s)\right) \frac{e^{-\rho\sqrt{s}}}{\rho}$$

which verifies condition (15).

Introducing (20) in (19) and from condition (16) we get the expression of $M_2(s)$

$$M_2(s) = -\frac{1-e^{-s\Delta\xi}}{2s\sqrt{s}}\, e^{2\sqrt{s}} \int_1^\infty \frac{e^{-u\sqrt{s}}}{u^3}\, du - B\frac{e^{\sqrt{s}}}{s}. \tag{21}$$

Then, the solution of (14)-(16) is

$$D(\rho,s) = \frac{1-e^{-s\Delta\xi}}{2\rho}\left(\int_1^\infty \frac{e^{-|u-\rho|\sqrt{s}}}{s\sqrt{s}}\,\frac{du}{u^3} - \int_1^\infty \frac{e^{-(u+\rho-2)\sqrt{s}}}{s\sqrt{s}}\,\frac{du}{u^3}\right) - \frac{Be^{-(\rho-1)\sqrt{s}}}{s\rho} \tag{22}$$

In order to obtain the solution of the problem, $V(\rho,\xi)$, we have to make the inverse Laplace transform of function $D(\rho,s)$. If $Erfc(x) = \frac{2}{\sqrt{\pi}}\int_x^\infty e^{-w^2}dw$ is the complementary error function, then

$$\mathcal{L}^{-1}\left[\frac{e^{-\phi\sqrt{s}}}{s\sqrt{s}}\right] = \frac{2\sqrt{\xi}}{\sqrt{\pi}}\, e^{-\frac{\phi^2}{4\xi}} - \phi\, Erfc\left(\frac{\phi}{2\sqrt{\xi}}\right) \tag{23}$$

$$\mathcal{L}^{-1}\left[\frac{e^{-\phi\sqrt{s}}}{s}\right] = Erfc\left(\frac{\phi}{2\sqrt{\xi}}\right). \tag{24}$$

Using (23) for $\phi = |u-\rho|$ and $\phi = u+\rho-2$, we denote

$$V_1(\rho,\xi) = \int_1^\infty \left(\frac{2\sqrt{\xi}}{\sqrt{\pi}} e^{-\frac{(u-\rho)^2}{4\xi}} - |u-\rho| Erfc\left(\frac{|u-\rho|}{2\sqrt{\xi}}\right)\right)\frac{du}{2\rho u^3}$$

$$V_2(\rho,\xi) = \int_1^\infty \left(\frac{2\sqrt{\xi}}{\sqrt{\pi}} e^{-\frac{(u+\rho-2)^2}{4\xi}} - (u+\rho-2) Erfc\left(\frac{u+\rho-2}{2\sqrt{\xi}}\right)\right)\frac{du}{2\rho u^3}$$

And from (24), for $\phi = \rho - 1$, we denote

$$V_3(\rho,\xi) = \frac{B}{\rho}\, Erfc\left(\frac{\rho-1}{2\sqrt{\xi}}\right).$$

Taking into account that if $\mathcal{L}^{-1}[f(s)] = F(t)$, then $\mathcal{L}^{-1}[e^{-as}f(s)] = H(t-a)F(t-a)$ the solution of problem is

$$V(\rho,\xi) = V_1(\rho,\xi) - V_2(\rho,\xi) - H(\xi-\Delta\xi)(V_1(\rho,\xi-\Delta\xi) - V_2(\rho,\xi-\Delta\xi)) - V_3(\rho,\xi).$$

3.2. **Case B: Dirichlet boundary condition and modeling a pre-cooling period.** In this case the problem consists of finding the solution of the governing equation (2) with the boundary conditions (4) and (6). The initial condition we need is established considering the stationary problem from equation (8):

$$T''(r) + \frac{2}{r}T'(r) = 0\,; \qquad T(r_0) = T_c\,; \qquad \lim_{r\to\infty} T(r) = T_0\,. \tag{25}$$

The solution of this problem

$$T(r) = \frac{r_0(T_c - T_0)}{r} + T_0 \tag{26}$$

is now the initial condition. According to the changes established in (9) the problem is

$$-\left(\frac{\partial^2 V}{\partial\rho^2}(\rho,\xi) + \frac{2}{\rho}\frac{\partial V}{\partial\rho}(\rho,\xi)\right) + \frac{\partial V}{\partial\xi}(\rho,\xi) = \frac{1}{\rho^4}(H(\xi) - H(\xi-\Delta\xi)) \tag{27}$$

$$V(\rho,0) = -\frac{B}{\rho} \qquad \forall\,\rho > 1 \tag{28}$$

$$\lim_{\rho\to\infty} V(\rho,\xi) = 0 \qquad \forall\,\xi > 0 \tag{29}$$

$$V(1,\xi) = -B \qquad \forall\,\xi > 0\,. \tag{30}$$

Again, taking Laplace transform respect to $\xi$ and denoting $D(\rho,s) := \mathcal{L}(V(\rho,\xi))$ we get

$$-\left(\frac{\partial^2 D}{\partial\rho^2} + \frac{2}{\rho}\frac{\partial D}{\partial\rho}\right) + s\,D + \frac{B}{\rho} = \frac{1}{\rho^4}\left(\frac{1-e^{-s\Delta\xi}}{s}\right) \tag{31}$$

$$\lim_{\rho\to\infty} D(\rho,s) = 0 \tag{32}$$

$$D(1,s) = -\frac{B}{s}\,. \tag{33}$$

Note that in this case equation (31) has an additional term, $B/\rho$.

Following the same steps than in Case A we get the general solution of the problem (31)-(33)

$$\begin{aligned} D(\rho,s) =& \frac{e^{\rho\sqrt{s}}}{\rho}\left(\int_1^\rho \frac{e^{-u\sqrt{s}}}{2\sqrt{s}}\left(B - \frac{1-e^{-s\Delta\xi}}{su^3}\right)du + M_1(s)\right) + \\ & \frac{e^{-\rho\sqrt{s}}}{\rho}\left(\int_1^\rho \frac{e^{u\sqrt{s}}}{2\sqrt{s}}\left(B - \frac{1-e^{-s\Delta\xi}}{su^3}\right)du + M_2(s)\right). \end{aligned} \tag{34}$$

From condition (32), as in the previous case, we have to determine $M_1(s)$ in order to verify

$$\lim_{\rho\to\infty} \frac{e^{\rho\sqrt{s}}}{\rho}\left(\int_1^\rho \frac{e^{-u\sqrt{s}}}{2\sqrt{s}}\left(B - \frac{1-e^{-s\Delta\xi}}{su^3}\right)du + M_1(s)\right) = 0\,.$$

Since

$$\int_1^\rho \frac{e^{-u\sqrt{s}}}{\sqrt{s}}\,du = \frac{e^{-\sqrt{s}} - e^{-\rho\sqrt{s}}}{s}$$

we get

$$M_1(s) = (1 - e^{-s\Delta\xi}) \int_1^\infty \frac{e^{-u\sqrt{s}}}{2s\sqrt{s}} \frac{du}{u^3} - \frac{Be^{-\sqrt{s}}}{2s} , \tag{35}$$

and in this way

$$D(\rho, s) = -\frac{B(2 - e^{-(\rho-1)\sqrt{s}})}{2s\rho} + \frac{M_2(s)e^{-\rho\sqrt{s}}}{\rho} + \frac{1 - e^{-s\Delta\xi}}{2\rho} \left( \int_\rho^\infty \frac{e^{-(u-\rho)\sqrt{s}}}{s\sqrt{s}} \frac{du}{u^3} + \int_1^\rho \frac{e^{-(\rho-u)\sqrt{s}}}{s\sqrt{s}} \frac{du}{u^3} \right) . \tag{36}$$

Introducing (35) in (34), from condition (33) we obtain

$$M_2(s) = -\frac{Be^{\sqrt{s}}}{2s} - \frac{e^{\sqrt{s}}(1 - e^{-s\Delta\xi})}{2} \int_1^\infty \frac{e^{-(u-1)\sqrt{s}}}{s\sqrt{s}} \frac{du}{u^3} . \tag{37}$$

Then, the solution of (31)-(33) is

$$D(\rho, s) = -\frac{B}{s\rho} + \frac{1 - e^{-s\Delta\xi}}{2\rho} \left( \int_1^\infty \frac{e^{-|u-\rho|\sqrt{s}}}{s\sqrt{s}} \frac{du}{u^3} - \int_1^\infty \frac{e^{-(u+\rho-2)\sqrt{s}}}{s\sqrt{s}} \frac{du}{u^3} \right) .$$

The Laplace inverse transform of $D(\rho, s)$ is made using (23) and (24) in the same way than in Case A. Finally, the dimensionless temperature

$$V(\rho, \xi) = V_1(\rho, \xi) - V_2(\rho, \xi) - H(\xi - \Delta\xi)(V_1(\rho, \xi - \Delta\xi) - V_2(\rho, \xi - \Delta\xi)) - \frac{B}{\rho} .$$

3.3. **Case C: Boundary condition based on Newton's cooling law and uniform initial condition.** In this section the problem consists of finding the solution of the governing equation (2) taking into account the initial condition (7) and the boundary conditions (5) and (6).

To simplify the solution of the problem we make the change of variables of (9). In this way the resulting problem is

$$-\left( \frac{\partial^2 V}{\partial \rho^2}(\rho, \xi) + \frac{2}{\rho} \frac{\partial V}{\partial \rho}(\rho, \xi) \right) + \frac{\partial V}{\partial \xi}(\rho, \xi) = \frac{1}{\rho^4} (H(\xi) - H(\xi - \Delta\xi)) \tag{38}$$

$$V(\rho, 0) = 0 \qquad \forall\, \rho > 1 \tag{39}$$

$$\lim_{\rho \to \infty} V(\rho, \xi) = 0 \qquad \forall\, \xi > 0 \tag{40}$$

$$p\, \frac{\partial V}{\partial \rho}(1, \xi) - V(1, \xi) - B = 0 \qquad \forall\, \xi > 0 \tag{41}$$

where $p = \frac{k}{hr_0}$.

Taking Laplace transform respect to $\xi$ and denoting $D(\rho, s) := \mathcal{L}(V(\rho, \xi))$ we get

$$-\left( \frac{\partial^2 D}{\partial \rho^2} + \frac{2}{\rho} \frac{\partial D}{\partial \rho} \right) + s\, D = \frac{1}{\rho^4} \left( \frac{1 - e^{-s\Delta\xi}}{s} \right) \tag{42}$$

$$\lim_{\rho \to \infty} D(\rho, s) = 0 \tag{43}$$

$$-D(1, s) + p\, \frac{\partial D}{\partial \rho}(1, s) - \frac{B}{s} = 0 . \tag{44}$$

As equation (42) and condition (43) are the same than in Case A, following the same steps than in that section we get

$$D(\rho,s)=\left(\frac{1-e^{-\Delta\xi s}}{2s\sqrt{s}}\int_{\rho}^{\infty}\frac{e^{-u\sqrt{s}}}{u^3}\,du\right)\frac{e^{\rho\sqrt{s}}}{\rho}+\left(\frac{1-e^{-\Delta\xi s}}{2s\sqrt{s}}\int_{1}^{\rho}\frac{e^{u\sqrt{s}}}{u^3}\,du+M_2(s)\right)\frac{e^{-\rho\sqrt{s}}}{\rho}\,.$$

$M_2(s)$ is obtained using condition (44)

$$M_2(s)=\frac{1-e^{-s\Delta\xi}}{2s\sqrt{s}}\,e^{2\sqrt{s}}\,\frac{p\,(\sqrt{s}-1)-1}{p\,(\sqrt{s}+1)+1}\int_{1}^{\infty}\frac{e^{-u\sqrt{s}}}{u^3}du-\frac{B\,e^{\sqrt{s}}}{s\,(p\,(\sqrt{s}+1)+1)}\,.$$

In this way the solution of (42)-(44) is

$$D(\rho,s)=\frac{1-e^{-s\Delta\xi}}{2\rho}\left(\int_{1}^{\infty}\frac{e^{-|u-\rho|\sqrt{s}}}{s\sqrt{s}}\frac{du}{u^3}-\int_{1}^{\infty}\frac{e^{-(u+\rho-2)\sqrt{s}}}{s\sqrt{s}}\frac{du}{u^3}+\int_{1}^{\infty}\frac{2\,p\,e^{-(u+\rho-2)\sqrt{s}}}{s\,(p\,(\sqrt{s}+1)+1)}\frac{du}{u^3}\right)-\frac{B\,e^{-(\rho-1)\,\sqrt{s}}}{\rho s\,(p\,(\sqrt{s}+1)+1)}\,.$$

The Laplace inverse transform of the first and second term of $D(\rho,s)$ is made using (23) and (24) in the same way than in Case A. In order to make the other terms Laplace inverse transform we use the formula:

$$\mathcal{L}^{-1}\left[\frac{e^{-\phi\sqrt{s}}}{s(\sqrt{s}+\beta)}\right]=\frac{1}{\beta}\left(Erfc\left(\frac{\phi}{2\sqrt{\xi}}\right)-e^{\beta(\phi+\beta\xi)}Erfc\left(\frac{\phi}{2\sqrt{\xi}}+\beta\sqrt{\xi}\right)\right).\quad(45)$$

Using (45) for $\phi=u+\rho-2$ and $\beta=a=1+\frac{1}{p}$, we denote

$$V_4(\rho,\xi)=\frac{1}{a\rho}\int_{1}^{\infty}\left(Erfc\left(\frac{u+\rho-2}{2\sqrt{\xi}}\right)-e^{a(a\xi+\rho-1)}Erfc\left(a\sqrt{\xi}+\frac{u+\rho-2}{2\sqrt{\xi}}\right)\right)\frac{du}{u^3}.$$

And from (45) for $\beta=a=1+\frac{1}{p}$ and $\phi=\rho-1$ we denote

$$V_5(\rho,\xi)=\frac{B}{\rho\,p\,a}\left(Erfc\left(\frac{\rho-1}{2\sqrt{\xi}}\right)-e^{a(a\xi+\rho-1)}Erfc\left(a\sqrt{\xi}+\frac{\rho-1}{2\sqrt{\xi}}\right)\right)\,.$$

In this way the solution of the problem is

$$V(\rho,\xi)=V_1(\rho,\xi)-V_2(\rho,\xi)+V_4(\rho,\xi)-H(\xi-\Delta\xi)\,(V_1(\rho,\xi-\Delta\xi)-V_2(\rho,\xi-\Delta\xi)+V_4(\rho,\xi-\Delta\xi))-V_5(\rho,\xi)\,.$$

3.4. **Case D: Boundary condition based on Newton's cooling law and modeling a pre-cooling period.** In this section our problem is formulated considering the governing equation (2) and the boundary conditions (5) and (6) like in Case B. Moreover, now the initial condition is established considering the stationary problem from equation (8):

$$T''(r)+\frac{2}{r}\,T'(r)=0\,;\qquad\lim_{r\to\infty}T(r)=T_0\,;\qquad -k\,T'(r_0)=h\,(T_c-T(r_0))\,.\quad(46)$$

The solution of this problem

$$T(r) = -\frac{r_0^2\, h\, (T_0 - T_c)}{(k + hr_0)\, r} + T_0 \tag{47}$$

is now the initial condition we need.

According to the changes made in (9) the problem we want to solve is

$$-\left(\frac{\partial^2 V}{\partial \rho^2}(\rho,\xi) + \frac{2}{\rho}\frac{\partial V}{\partial \rho}(\rho,\xi)\right) + \frac{\partial V}{\partial \xi}(\rho,\xi) = \frac{1}{\rho^4}\left(H(\xi) - H(\xi - \Delta\xi)\right) \tag{48}$$

$$V(\rho,0) = -\frac{B\, q}{\rho} \qquad \forall\, \rho > 1 \tag{49}$$

$$\lim_{\rho\to\infty} V(\rho,\xi) = 0 \qquad \forall\, \xi > 0 \tag{50}$$

$$p\, \frac{\partial V}{\partial \rho}(1,\xi) - V(1,\xi) - B = 0 \qquad \forall\, \xi > 0 \tag{51}$$

where $q = \frac{r_0\, h}{k + h\, r_0}$.

Taking Laplace transform respect to $\xi$ and denoting $D(\rho,s) := \mathcal{L}(V(\rho,\xi))$ we get

$$-\left(\frac{\partial^2 D}{\partial \rho^2} + \frac{2}{\rho}\frac{\partial D}{\partial \rho}\right) + s\, D + \frac{B\, q}{\rho} = \frac{1}{\rho^4}\left(\frac{1 - e^{-s\Delta\xi}}{s}\right) \tag{52}$$

$$\lim_{\rho\to\infty} D(\rho,s) = 0 \tag{53}$$

$$-D(1,s) + p\, \frac{\partial D}{\partial \rho}\,(1,s) - \frac{B}{s} = 0\,. \tag{54}$$

Equation (52) is similar to (31), and condition (53) is the same than (32). Then, following the same steps than in Case B we obtain the general solution of problem (52)-(54)

$$\begin{aligned} D(\rho,s) =& \frac{e^{\rho\sqrt{s}}}{\rho}\left(\int_1^\rho \frac{e^{-u\sqrt{s}}}{2\sqrt{s}}\left(Bq - \frac{1 - e^{-s\Delta\xi}}{su^3}\right) du + M_1(s)\right) + \\ & \frac{e^{-\rho\sqrt{s}}}{\rho}\left(-\int_1^\rho \frac{e^{u\sqrt{s}}}{2\sqrt{s}}\left(Bq - \frac{1 - e^{-s\Delta\xi}}{su^3}\right) du + M_2(s)\right)\,. \end{aligned} \tag{55}$$

where

$$M_1(s) = (1 - e^{-s\Delta\xi})\int_1^\infty \frac{e^{-u\sqrt{s}}}{2s\sqrt{s}}\frac{du}{u^3} - \frac{B\, q e^{-\sqrt{s}}}{2s}\,. \tag{56}$$

Introducing (56) in (55) and from condition (54) we obtain

$$\begin{aligned} M_2(s) =& \frac{1 - e^{-s\Delta\xi}}{2s\sqrt{s}}\, e^{2\sqrt{s}}\, \frac{p\,(\sqrt{s} - 1) - 1}{p\,(\sqrt{s} + 1) + 1}\int_1^\infty \frac{e^{-u\sqrt{s}}}{u^3}\, du \\ & - \frac{B\, q\, e^{\sqrt{s}}}{2s} + \frac{B\,(q(p+1) - 1)\, e^{\sqrt{s}}}{s\,(p\,(\sqrt{s} + 1) + 1)}\,. \end{aligned}$$

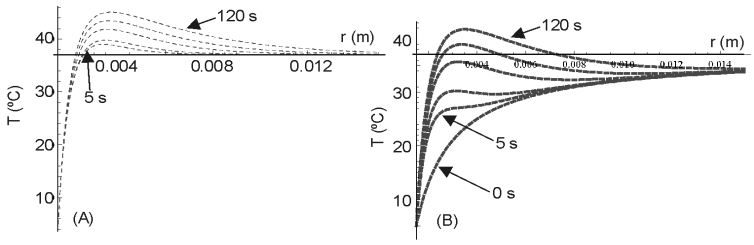


FIGURE 2. Temperature profiles during RF application (120 s) for Dirichlet thermal boundary conditions at the electrode-tissue interface. A: without considering a pre-cooling period (plots correspond with 5, 10, 30, 60 and 120 s); B: considering a pre-cooling period (plots correspond with 0, 5, 10, 30, 60 and 120 s). $x$-axis starts at $r_0$.

Putting the expressions of $M_1(s)$ and $M_2(s)$ into (55) and taking into account that $(p+1)q-1=0$ we get

$$D(\rho,s) = \frac{1-e^{-s\Delta\xi}}{2\rho}\left(\int_1^\infty \frac{e^{-|u-\rho|\sqrt{s}}}{s\sqrt{s}}\,\frac{du}{u^3} - \int_1^\infty \frac{e^{-(u+\rho-2)\sqrt{s}}}{s\sqrt{s}}\,\frac{du}{u^3} + \int_1^\infty \frac{2\,p\,e^{-(u+\rho-2)\sqrt{s}}}{s\,(p\,(\sqrt{s}+1)+1)}\,\frac{du}{u^3}\right) - \frac{B\,q}{s\,\rho}\,.$$

We have made the computation of the Laplace inverse transform of all the terms in $D(\rho,s)$ in the previous sections. In this way, the solution of the problem (48)-(51) is

$$V(\rho,\xi) = V_1(\rho,\xi) - V_2(\rho,\xi) + V_4(\rho,\xi) - H(\xi-\Delta\xi)(V_1(\rho,\xi-\Delta\xi) - V_2(\rho,\xi-\Delta\xi) + V_4(\rho,\xi-\Delta\xi)) - \frac{q\,B}{\rho}.$$

4. **Computer results.** Figure 2 shows temperature profiles during RF application for Dirichlet thermal boundary conditions at the electrode-tissue interface. The results show that the profiles obtained with and without pre-cooling are very similar for a long time (120 s). However, for shorter times ($<30$ s), the Case A model (i.e. without pre-cooling) overestimates the temperature, specially at points away from the electrode-tissue interface. In fact, the temperature at the interface is very similar for both models (Cases A and B) at all times. On the other hand, we observed a clear disagreement between these cases when $r\to\infty$: in Case A, the temperature profiles tend towards $T_0$ from higher values. In contrast, in Case B, this tendency occurs from lower values. This behavior is also observed in Figure 3 which shows the temperature profiles after RF application. Moreover, during this period of post-RF application Case A slightly overestimates the temperature at points away from the electrode-tissue interface.

Figure 4 shows the temperature profiles during RF application for a boundary thermal condition at the electrode-tissue interface based on Newton's cooling law.

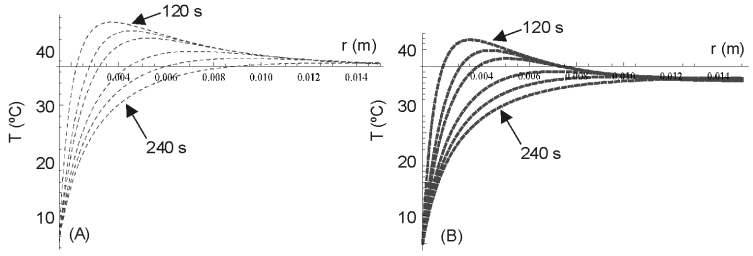


FIGURE 3. Temperature profiles after RF application (120 s) for Dirichlet thermal boundary conditions at the electrode-tissue interface. A: without considering a pre-cooling period; B: considering a pre-cooling period. Plots correspond with 120, 125, 130, 150, 180 and 240 s. $x$-axis starts at $r_0$.

Once more, the most noticeable result is the overestimation in the computed temperature at points away from the electrode-tissue interface when the pre-cooling period is not considered (Case C versus D), especially for shorter times. This disagreement is more evident for higher $h$ values. Regarding the temperature profiles after RF application (see Fig. 5), the disagreements between Cases C and D are smaller than during the heating phase. Once more, the non pre-cooling case (Case C) slightly overestimates the temperature at points away from the electrode-tissue interface.

On the other hand, on comparing Dirichlet boundary conditions (Cases A and B) to those associated with Newton's cooling law (Cases C and D), we observed that when the convective heat transfer coefficient ($h$) is increased in Cases C and D, the temperature profiles obtained become more similar to those from Dirichlet's solution. However, for the range of $h$ values considered in our study ($1000 - 4000$ W/m$^2$K) the temperature profiles obtained in Cases A and B (Dirichlet) are significantly lower than those obtained in Cases C and D.

We also conducted computer simulations varying coolant temperature $T_c$ between 5 and 20 °C [9]. The results showed that with at higher coolant temperature, temperature profiles are usually slightly higher. Figure 6 shows the temperature profiles at 120 s for the four boundary conditions considered and for three values of coolant temperature.

Finally, in order to obtain conclusions from a clinical point of view, we plotted the time progress of maximal tissue temperature $T_{max}$ and temperature at the tip of the cooled electrode ($T_{tip}$, at $r = r_0$) (Fig. 7). Figure 7 shows the time progress of the depth (distance from the electrode surface) at which $T_{max}$ was registered. These parameters are important since, on one hand, $T_{tip}$ can be measured when cooled electrodes are employed clinically, and on the other, both $T_{max}$ and its location could be used as indicators of lesion depth. Regarding the effect of the convective heat transfer coefficient $h$ (which models the internal flow rate), we observed that lower values bring about higher $T_{tip}$ and $T_{max}$ temperatures. In contrast, $T_{max}$ depth increases with $h$ (i.e. with higher internal flow rates). However, the shift of $T_{max}$ inside the tissue does not automatically imply increased lesion size (assessed, for instance, by using the 50 °C isotherm), due to the temperatures here being considerably lower at high $h$ values (see Fig. 7).

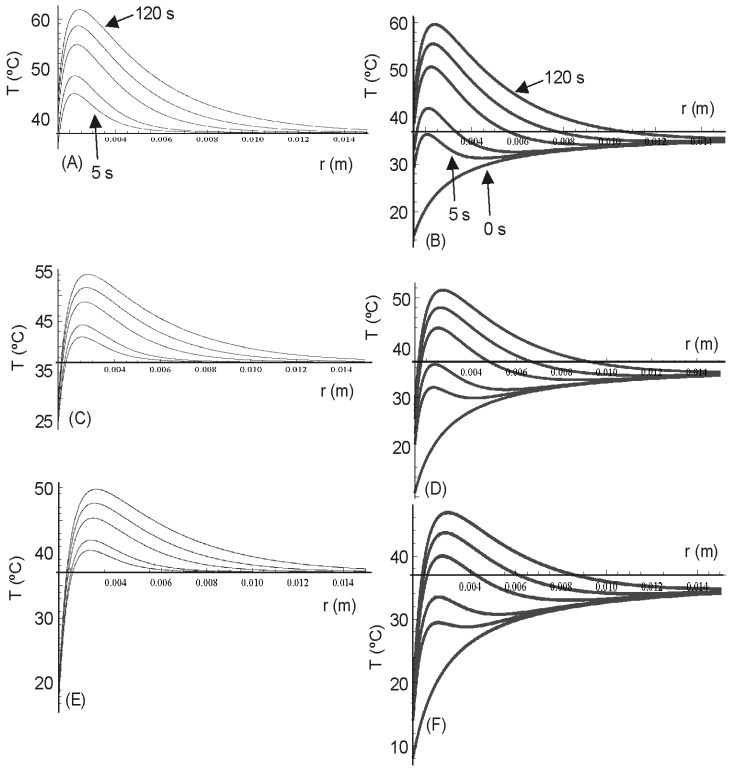


FIGURE 4. Temperature profiles during RF application (120 s) for boundary condition at the electrode-tissue interface based on Newton's cooling law with different values of convective heat transfer coefficient: 1000 W/m$^2$K (A and B), 2000 W/m$^2$K (C and D), and 4000 W/m$^2$K (E and F). Figures A, C and E are without pre-cooling period (plots correspond with 5, 10, 30, 60 and 120 s). Figures B, D and F are with pre-cooling period (plots correspond with 0, 5, 10, 30, 60 and 120 s). $x$-axis starts at $r_0$.

5. **Discussion.** This study was conducted to compare the temperature profiles obtained during RF ablation with cooled electrodes when different thermal boundary conditions at the electrode-tissue interface are considered. We chose an analytical approach similar to that proposed by Erez and Shitzer [7] for a dry electrode. We then modified this model by changing the thermal boundary condition at the interface. We also solved the time-dependence of the heat source in the governing equation, which not only provide the temperature profile during the heating phase (RF application) but also during the subsequent cooling phase (after RF application). In this aspect, our study offers an improvement on the previously published analytical model [7].

Previous RF cardiac ablation modeling studies with cooled electrodes employed a Dirichlet thermal boundary condition [11, 14] and did not consider any pre-cooling period. Our results indicate that, whatever the type of boundary condition, this

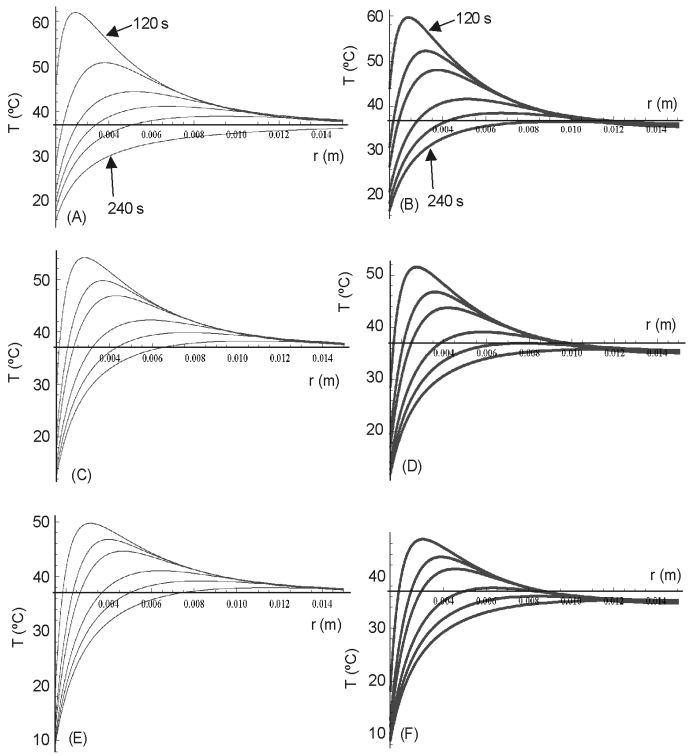


FIGURE 5. Temperature profiles after RF application (120 s pulse) for boundary condition at the electrode-tissue interface based on Newton's cooling law with different values of convective heat transfer coefficient: 1000 W/m$^2$K (A and B), 2000 W/m$^2$K (C and D), and 4000 W/m$^2$K (E and F). Figures A, C and E are without pre-cooling period. Figures B, D and F are with pre-cooling period. Plots correspond with 120, 125, 130, 150, 180 and 240 s. $x$-axis starts at $r_0$.

period should be included in the modeling, especially if temperature profiles for initial RF application ($< 30$ s) are under study.

It should also be borne in mind that if a cooled electrode is programmed with low flow in the internal circuit, i.e. when a low $h$ value is involved, the thermal profiles obtained from Dirichlet and Newton's cooling law could be very different. In fact, using a Dirichlet condition, the temperature at the electrode is always fixed by to coolant temperature, something which is not observed in a real situation [19, 2], when electrode temperature is seen to increase during ablation.

Our computer simulations also considered the effect of varying coolant temperature $T_c$. Such as shown in Figure 6, temperature profile values rose with $T_c$. This finding is not in agreement with that obtained by Haemmerich *et al* [9] in an RF hepatic ablation analytical model. They observed that $T_c$ did not have any effect on temperature profiles [9]. However, our results are not directly comparable to the results obtained by these authors, since they only solved the steady-state solution

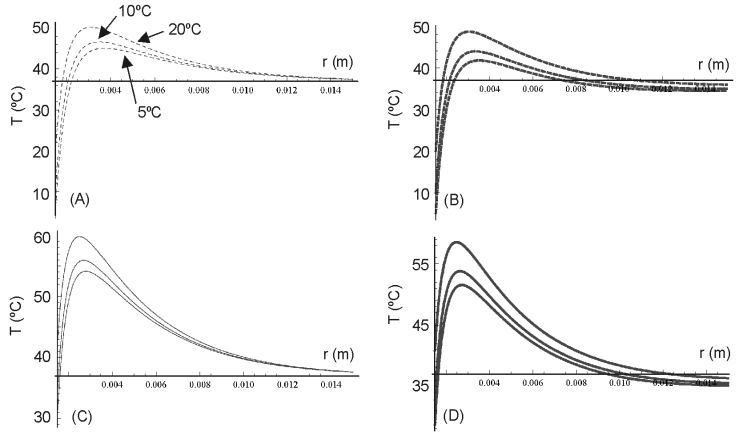


FIGURE 6. Effect of coolant temperature $T_c$ on the temperature profiles at 120 s. Three values of $T_c$ are shown (5, 10 and 20 °C) for the four boundary conditions at the electrode-tissue interface: Dirichlet condition without (A) and with pre-cooling period (B); and the condition based on Newton's cooling law without (C) and with pre-cooling period (D). In this case a value of 2000 W/m$^2$°C was employed for convective heat transfer coefficient.

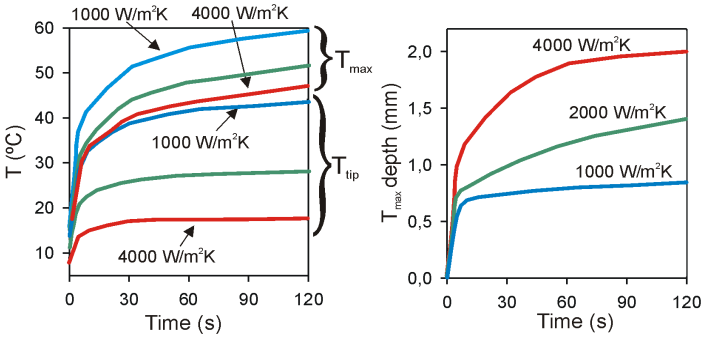


FIGURE 7. Left: Time progress of maximal temperature reached in the tissue $T_{max}$ and temperature measured at the tip of the cooled electrode ($T_{tip}$, at $r = r_0$) for the case D (boundary condition based on Newton's cooling law and modeling a pre-cooling period). Right: Time progress of $T_{max}$ location (assessed as distance from electrode surface). $T_{max}$ was considered to be the relative maximum temperature reached near the electrode surface, and hence, before RF was applied, this value was even lower than the temperature of the non heated tissue ($T_0 = 37$ °C). The plots shown three cases of values of convective heat transfer coefficient $h$: 1000, 2000 and 4000 W/m$^2$°C.

in cylindrical geometry, which is very different case to our model. Finally, we also verified (data not shown) that the value of $T_c$ did not influence the conclusions reached concerning the different boundary conditions obtained in our study.

Regarding the computer simulations of the time progress of $T_{tip}$ and $T_{max}$, our results indicate that both values are directly related to each other. In fact, this behavior could be useful during RF cardiac ablation if the RF power is modulated to achieve $T_{tip}$ of 40 °C, which has been defined as the approximate upper safety limit [5]. Our results also suggest that internal flow rate (i.e. parameter $h$) has a strong influence on temperature profile, in particular on the value of $T_{max}$ and its location. For instance, when a low flow rate is employed, temperatures are higher and $T_{max}$ is located closer to the electrode surface. The limit situation of an extremely low flow rate would be a dry electrode (i.e. without internal cooling) with very similar $T_{tip}$ and $T_{max}$ values, so that $T_{max}$ would be located almost on the electrode surface.

Finally, on comparing our temperature profiles to those previously reported for dry electrodes (see Fig. 4 in [13]), we clearly observed the cooling effect at the electrode-tissue interface, and hence lower temperatures for the same conditions of applied power, tissue characteristics, electrode geometry and ablation time.

This analytical study has several limitations. The problem solved was linear, since no change of electrical conductivity with temperature was considered [1]. Taking this change into account, the analytical solution would become extremely complex. The electrode geometry (spherical) was not exactly the same as a real electrode (hemispherical), nor did we include the cooling effect of blood circulating around part of the electrode surface. In spite of these limitations, we think that the conclusions of this study should be taken into account not only in modeling studies of RF cardiac ablation, but also in other RF ablation modeling studies using cooled electrodes, such as tumor ablation [6, 9].

6. **Conclusions.** Theoretical modeling of RF ablation using internally cooled electrodes should consider: 1) a thermal boundary condition (at the electrode-tissue interface) based on Newton's cooling law rather than a Dirichlet condition, especially for low flow in the internal circuit; and 2) the modeling of a pre-cooling period, especially if one is interested in the thermal profiles registered in the initial period of RF application. We verified that these conclusions remained true for coolant temperatures values between 5 and 20 °C.

**Acknowledgments.** We would like to thank the R&D&I Linguistic Assistance Office, Universidad Politécnica de Valencia (Spain), for granting financial support for the linguistic revision of this paper.

## REFERENCES

[1] E. J. Berjano, *Theoretical modeling for radiofrequency ablation: State-of-the-art and challenges for the future* Biomed. Eng. Online, **18** (2006), 5–24.

[2] G. K. Bruce, T. J. Bunch, M. A. Milton, A. Sarabanda, S. B. Johnson and D. L. Packer, *Discrepancies between catheter tip and tissue temperature in cooled-tip ablation: Relevance to guiding left atrial ablation*, Circulation, **112** (2005), 954–960.

[3] F. Burdío, E. J. Berjano, A. Navarro, J. M. Burdío, A. Güemes, L. Grande, R. Sousa, J. Subiró, A. Gonzalez, I. Cruz, T. Castiella, E. Tejero, R. Lozano and M. A. de Gregorio, *RF tumor ablation with internally cooled electrodes and saline infusion: What is the optimal location of the saline infusion?,* Biomed. Eng. Online, **16** (2007), 6–30.

[4] A. D'Avila, C. Houghtaling, P. Gutierrez, O. Vragovic, J. N. Ruskin, M. E. Josephson and V. Y. Reddy, *Catheter ablation of ventricular epicardial tissue: A comparison of standard and cooled-tip radiofrequency energy*, Circulation, **109** (2004), 2363–2369.

[5] J. M. Cooper, J. L. Sapp, D. Robinson, L. M. Epstein and W. G. Stevenson, *A rewarming maneuver demonstrates the contribution of blood flow to electrode cooling during internally irrigated RF ablation*, J. Cardiovasc. Electrophysiol., **19** (2008), 409–414.

[6] V. Ekstrand, H. Wiksell, I. Schultz, B. Sandstedt, S. Rotstein and A. Eriksson, *Influence of electrical and thermal properties on RF ablation of breast cancer: Is the tumour preferentially heated?*, Biomed. Eng. Online,**11** (2005), 4–41.

[7] A. Erez and A. Shitzer, *Controlled destruction and temperature distributions in biological tissues subjected to monoactive electrocoagulation*, J. Biomech. Eng., **102** (1980), 42–49.

[8] J. Gopalakrishnan, *A mathematical model for irrigated epicardial radiofrequency ablation*, Ann. Biomed. Eng., **30** (2002), 884–893.

[9] D. Haemmerich, L. Chachati, A. S. Wright, D. M. Mahvi, F. T. Lee Jr and J. G. Webster JG, *Hepatic radiofrequency ablation with internally cooled probes: Effect of coolant temperature on lesion size*, IEEE Trans. Biomed. Eng., **50** (2003), 493–500.

[10] D. Haemmerich and B. J. Wood, *Hepatic radiofrequency ablation at low frequencies preferentially heats tumour tissue*, Int. J. Hyperthermia, **22** (2006), 563–574.

[11] M. K. Jain, P. D. Wolf and C. Henriquez, *Chilled-tip electrode radio frequency ablation of the endocardium: a finite element study*, Engineering in Medicine and Biology Society, IEEE 17th Annual Conference, **1** (1995), 273–274.

[12] J. M. Lee, J. K. Han, J. M. Chang, S. Y. Chung, S. H. Kim, J. Y. Lee and B. I. Choi, *Radiofrequency ablation in pig lungs: In vivo comparison of internally cooled, perfusion and multitined expandable electrodes*, Br. J. Radiol., **79** (2006), 562–571.

[13] J. A. López-Molina, M. J. Rivera, M. Trujillo, F. Burdio, J. L. Lequerica, F. Hornero and E. J. Berjano, *Assessment of hyperbolic heat transfer equation in theoretical modeling for radiofrequency heating techniques*, Open Biomed. Eng. J., **2** (2008), 22–27.

[14] D. Panescu, S. D. Fleischman, J. G. Whayne and D. K. Swanson, *Temperature distribution under cooled electrodes during radiofrequency catheter ablation*, Engineering in Medicine and Biology Society, IEEE 17th Annual Conference, **1** (1995), 299–300.

[15] T. A. Pilcher, A. L. Sanford, J. P. Saul and D. Haemmerich, *Convective cooling effect on cooled-tip catheter compared to large-tip catheter radiofrequency ablation*, Pacing Clin. Electrophysiol., **29** (2006), 1368–1374.

[16] V. Quaranta, G. Manenti, F. Bolacchi, E. Cossu, C. A. Pistolese, O. C. Buonomo, L. Carotenuto, C. Piconi and G. Simonetti, *FEM analysis of RF breast ablation: Multiprobe versus cool-tip electrode*, Anticancer Res., **27** (2007), 775–784.

[17] T. Shibata, T. Shibata, Y. Maetani, H. Isoda and M. Hiraoka, *Radiofrequency ablation for small hepatocellular carcinoma: Prospective comparison of internally cooled electrode and expandable electrode*, Radiology, **238** (2006), 346–353.

[18] C. Welp, S. Siebers, H. Ermert and J. Werner, *Investigation of the influence of blood flow rate on large vessel cooling in hepatic radiofrequency ablation*, Biomed. Tech. (Berl)., **51** (2006), 337–346.

[19] K. Yokoyama, H. Nakagawa, F. H. Wittkampf, J. V. Pitha, R. Lazzara and W. M. Jackman, *Comparison of electrode cooling between internal and open irrigation in radiofrequency ablation lesion depth and incidence of thrombus and steam pop*, Circulation, **113** (2006), 11–19.

Received September 15, 2008; Accepted February 5, 2009.

*E-mail address*: mjrivera@mat.upv.es
*E-mail address*: jalopez@mat.upv.es
*E-mail address*: matrugui@mat.upv.es
*E-mail address*: eberjano@eln.upv.es